Experimental Investigation of the Resistive-Wall Instability for Localized Perturbations in the Long-Wavelength Range

J. G. Wang, H. Suk, and M. Reiser
Institute for Plasma Research, University of Maryland, College Park, Maryland 20742
(Received 8 July 1996)

In high-current induction accelerators being considered for heavy ion inertial fusion and other applications, the resistive-wall instability in the long-wavelength range, may cause unacceptable beam energy spread. We have designed a small-scale low-cost electron beam experiment to investigate this instability in 1 m, 5–10 kΩ resistive-wall structures. In this Letter, we present the first experimental results on the interaction between a resistive wall and localized single space-charge waves in the long-wavelength range. The experiments have clearly demonstrated the growth of single slow waves due to the resistive-wall instability and the decay of single fast waves. The spatial growth/decay rates are measured and compared with theoretical analysis. [S0031-9007(97)03756-3]

PACS numbers: 29.27.Bd, 29.17.+w, 29.20.–c, 52.35.–g

The longitudinal instability of charged particle beams, caused by the growth of slow space-charge waves due to interaction with a dissipative wall, is an important issue in particle accelerators, microwave generators, and plasmas. The theoretical investigation of longitudinal velocity instabilities began long ago in the development of microwave tubes [1,2]. The amplification of longitudinal density fluctuations was first observed in an electron stream surrounded by a resistive wall by Birdsall *et al.* in 1953 [3]. This experiment was aimed at optimized high gain for microwave amplification in the short-wavelength range. The first theoretical work on the longitudinal resistive instability for intense coasting beams in particle accelerators was performed by Neil and Sessler in 1965 [4]. Following these early studies, considerable theoretical work has been done mainly for circular high-energy particle accelerators [5].

In recent years, the problem of longitudinal instabilities has received new attention in connection with research on high-current accelerators for various applications, such as the use of induction linear accelerators as drivers for heavy-ion inertial fusion. When the heavy ions are accelerated by induction gaps, the beam sees dissipative impedances. The interaction between the intense beam and the gap impedance causes longitudinal instability which may be detrimental to the beam. The instability in the long-wavelength range (wavelengths much longer than beam pipe circumferences) is a major potential problem. Though the growth rate of the resistive-wall instability in the long-wavelength range is quite low according to theory, the instability could still develop over distance in a long accelerator, and eventually deteriorate the beam quality. There have been extensive theoretical and computational investigations of the instability in the long-wavelength range, with regard, in particular, to heavy-ion fusion drivers [6–11]. But, there had been no experiment in this new parameter regime. Further, an experimental study of the instability with heavy-ion beams would be too difficult and too costly since a large-scale facility would be required in order to produce a measurable growth of the instability. This is evidenced by the conventional spatial growth rate formula for a pure resistive wall in the long-wavelength limit [12],

$$k_i = R_w^* \sqrt{\frac{\pi \varepsilon_0 q \Lambda_0}{g m \gamma}}, \tag{1}$$

which is a special case of the more general Eq. (2) to be discussed below. Here R_w^* is the wall resistance per unit length, Λ_0 is the beam line-charge density, q/m is the ratio of charge to mass of the particles, γ is the relativistic Lorentz factor, ε_0 is the permittivity of free space, and g is a geometry factor due to perturbations [13]. In a heavy-ion induction linac, an e-fold growth rate would require a machine hundreds of meters in length, according to Eq. (1).

We have designed an experiment to study the longitudinal instability in the long-wavelength range with electron beams [14]. By taking advantage of the small mass m of electrons, the large line-charge density Λ_0 in high current beams, and using a rather large wall resistance R_w^*, we are able to measure the instability growth rate in a small-scale low-cost facility. A novel and extremely useful feature in our experiments is the fact that we employ localized single space-charge waves for studying the resistive-wall interaction with the beam. Conventionally, the longitudinal instability has been studied with sinusoidal waves. This approach does not usually lead to a complete solution of the problem. In practice, perturbations to beams in accelerators are often in the form of localized short pulses. Thus, a time-domain approach based on localized perturbations in the experiment provides a better picture and a more realistic and complete analysis of the instability. In addition, this approach can avoid the problem of modulating long-wavelength sinusoidal signals on short bunched beams, and the problem of wave reflection at the bunch ends [15]. With single space-charge waves, the

 0031-9007/97/79(6)/1042(4)$10.00

interference between slow and fast waves in the interaction can be removed.

The experimental setup, as shown in Fig. 1, consists of a short-pulse electron beam injector, a resistive-wall channel, and diagnostics. The injector contains a gridded electron gun, which can produce the desired beam parameters with localized perturbations. The key component of the resistive-wall channel is a glass tube about 1 m in length and 3.81 cm in inner diameter. The inner surface of the glass tube is coated with indium-tin-oxide. Several such tubes have been custom-built for us at the Institute of Vacuum Electronics, Beijing. Two of the tubes with total resistances of 5.44 and 10.1 kΩ (correspond to 0.673 kΩ per square and 1.22 kΩ per square, respectively) are used in our experiments. The beam is focused by a 1.4 m long uniform solenoid coaxial to the resistive-wall tube. The magnetic field of the long solenoid is in the range of 46 to 80 G. Three short solenoidal lenses are employed in the injector to match the beam into this channel. The diagnostics include two fast wall-current monitors, one at the entrance and one at the exit of the resistive tube, to measure the beam-current signals with the perturbations. An axially movable phosphor screen in the diagnostic chamber could be used at the start of each experiment to check the beam image for the purpose of beam matching and centering. The beam parameters are in the range of 3–8 keV in energy, 25–140 mA in current, and about 100 ns in duration. Typical normalized beam emittance is 8.7 mm mrad. The matched beam diameters range from 0.6 to 1.2 cm.

In experiment, electron beams with localized perturbations are generated in the gridded electron gun and transported through the resistive-wall channel. By employing the technique described in a previous Letter [16], single slow or fast waves can be developed on these beam pulses. The perturbations are located in the center of the bunch, so that they do not reach the ends of the bunch after traveling through the channel. The interaction between the space-charge waves and the resistive wall leads to the instability, which can be diagnosed by the beam-current monitor signals. Figure 2 shows the growth of a single slow wave. It is clear from this figure that the amplitude of the slow wave is increased as expected. Similarly, Fig. 3 shows the decay of a localized fast wave after passing through the resistive-wall channel.

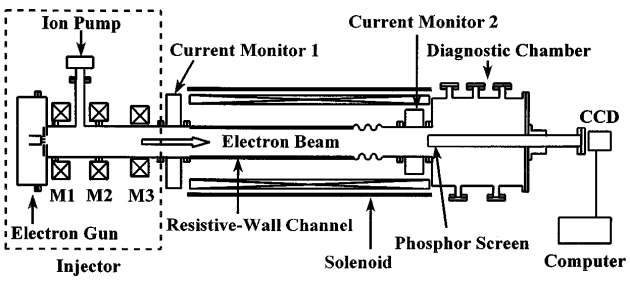

FIG. 1. Setup of the resistive-wall instability experiment.

Our theoretical work based on the frequency domain analysis shows that the spatial growth/decay rate k_i of the resistive-wall instability in the electrostatic long-wavelength range is given by [5,17]

$$k_i = \pm\left[\frac{\pi K\omega}{Z_0 c}\left(\sqrt{R_w^{*2} + X_s^{*2}} - X_s^*\right)\right]^{1/2}. \quad (2)$$

The (+) is for the growth rate of slow waves, while the (−) is for the decay rate of fast waves. Here $K = 2I/(I_0\gamma^3\beta^3)$ is the generalized perveance, with I being the beam current, I_0 being the characteristic current ($I_0 = 17$ kA for electrons), and $\beta = v/c$ being the relativistic velocity factor. In Eq. (2), $Z_0 = 1/\varepsilon_0 c = 377\ \Omega$ is the characteristic impedance of free space, ω is the perturbation frequency, and X_s^* is the space-charge wave impedance per unit length given by

$$X_s^* = \frac{gZ_0\omega}{4\pi c\beta^2\gamma^2}. \quad (3)$$

In the long-wavelength range the space-charge wave impedance is a linear function of the perturbation frequency, and the spatial growth rate of the instability also increases with the perturbation frequency. If the space-charge wave impedance is much larger than the wall resistance ($X_s^* \gg R_w^*$), the spatial growth rate formula, Eq. (2), reduces to Eq. (1), which gives the asymptotic value of the growth rate in the long-wavelength limit. The results from Eqs. (2) and (3) are depicted in Fig. 4, where the two horizontal lines represent the two tube resistances. At very low frequencies, the space-charge wave impedance is comparable to or even smaller than the wall resistance, so that the conventional growth rate formula in the long-wavelength limit, Eq. (1), overestimates the spatial growth rate.

For localized perturbations, the spectrum of space-charge waves covers a wide frequency range, starting

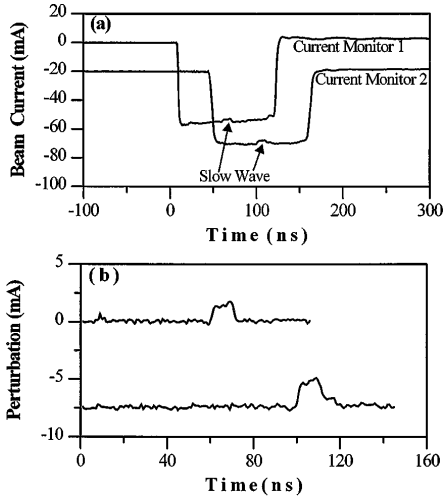

FIG. 2. Growth of a single slow wave in the resistive-wall channel, where (a) depicts the beam-current signals with a slow wave at the entrance and exit of the channel and (b) is the zoom-in view of the slow wave before and after the resistive channel.

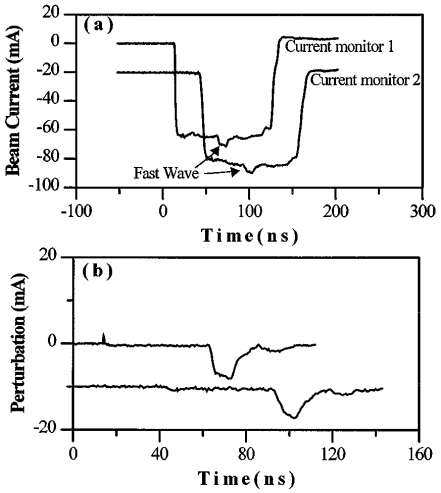

FIG. 3. Decay of a fast wave in the resistive-wall channel, where (b) is a zoom-in view of the fast wave in (a).

from zero up to a high limit determined by specific perturbation wave forms. In the experiments the "trapezoidal" perturbation wave form, shown in Figs. 2 and 3, is chosen since its flat-top shape satisfies basically the long-wavelength condition that makes it possible to compare the experiment and theory. The analysis shows that the frequency spectrum of the trapezoidal perturbation wave form is largely confined to the range within about 200 MHz, which corresponds to a space-charge wavelength of 21 cm for a 5 keV beam, in comparison to the pipe circumference of 12 cm. Though an insignificant power density of this spectrum extends to beyond 200 MHz, these frequency components affect mainly the rising and falling edges of the wave form. In terms of the amplitude of the trapezoidal perturbation wave form, i.e., the flat top rather than the edges, the long-wavelength condition is satisfied, so that Eq. (2) does apply. On the other hand, Eq. (1) overestimates the growth rate for very low frequency components of the spectrum since the space-charge wave impedance may be smaller than the wall resistance.

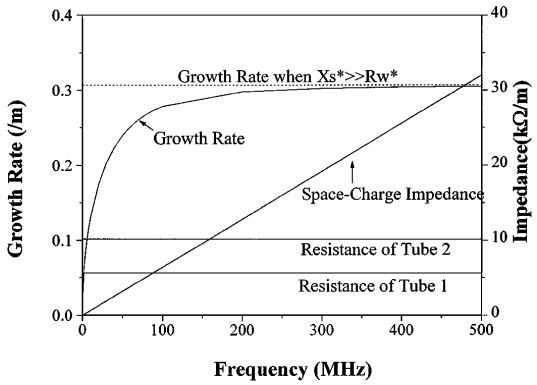

FIG. 4. Space-charge wave impedance and spatial growth rate vs perturbation frequency, where the calculation is done for a 5 keV, 60 mA beam with $R_w^* = 5.67\ \mathrm{k\Omega/m}$ and $g = 2$.

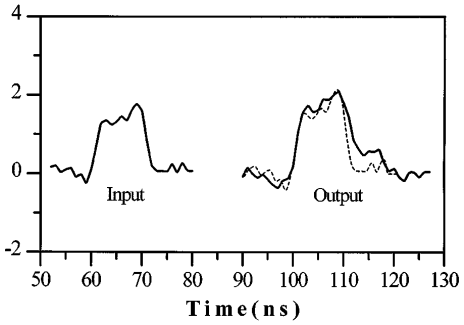

FIG. 5. Comparison between experiment and analysis for a slow wave, where solid wave forms are from experiment, while dashed output is from analysis.

In order to compare the experiment, which deals with localized perturbations in the time domain, with the theory based on the frequency domain analysis, we first find the frequency spectrum density of the measured input perturbation signal $h_i(t)$ at the entrance of the resistive channel by the Fourier transformation

$$H_i(\omega) = \frac{1}{\sqrt{2\pi}} \int h_i(t) e^{-i\omega t}\, dt\,. \tag{4}$$

We then calculate the output signal $h_0(t)$ at the exit of the channel by using the inverse Fourier transformation

$$h_0(t) = \frac{1}{\sqrt{2\pi}} \int H_i(\omega) e^{k_i(\omega)L} e^{i[\omega t - k_r(\omega)L]}\, d\omega\,, \tag{5}$$

where L is the length of the resistive tubes, and $k_r(\omega)$ is the perturbed wave number given by

$$k_r = \frac{\omega}{\beta c} \pm \left[\frac{\pi K \omega}{Z_0 c} \left(\sqrt{R_w^{*2} + X_s^{*2}} + X_s^* \right) \right]^{1/2}. \tag{6}$$

Here the $(-)$ applies to fast waves. The function $h_0(t)$ is compared with the measured output signal after the resistive wall.

In Fig. 5 we compare the experimental data for a slow wave with the analysis. Here the "input" depicts the experimental perturbation at the entrance of the channel. This signal is also digitized as the input $h_i(t)$ for analysis. The solid wave form in the "output" is the experimental perturbation signal at the exit of the channel. The dashed

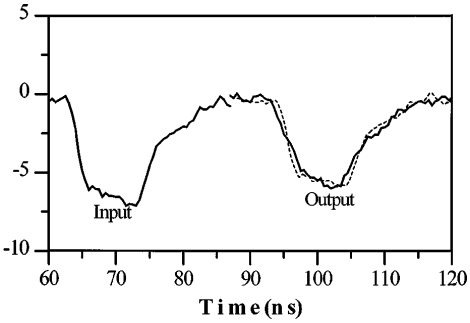

FIG. 6. Comparison between experiment and analysis for a fast wave, where solid wave forms are from experiment, while dashed output is from analysis.

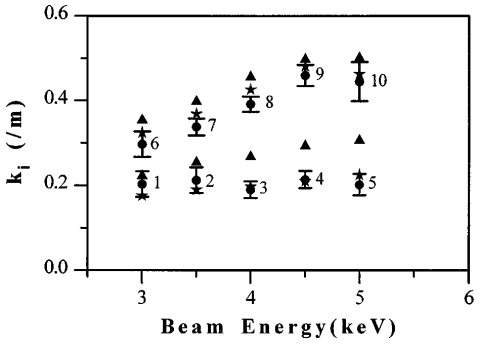

FIG. 7. Amplitude growth rate of slow waves with trapezoidal perturbation wave forms, where the dots with error bars represent the experimental results, the stars are from the Fourier analysis, and the triangles are from Eq. (1). The data points 1–5 are from the 5.44 kΩ tube, while the data points 6–10 are from the 10.1 kΩ tube.

wave form is $h_0(t)$, denoting the slow space-charge wave at the exit of the channel, as calculated from Eqs. (4)–(6). A similar comparison between the experiment and analysis for a fast wave is shown in Fig. 6, where the solid curve of the output is the fast wave from the experiment while the dashed curve is from the calculation. In both cases (slow and fast waves), there is good agreement between the experiment and the analysis in terms of the average wave amplitude. The difference on the edges of the perturbation wave forms is due to the effect of high frequency components beyond the long-wavelength limit in the perturbation signal, the effect of distributed capacitance along the resistive wall, and some reflections in the measured signal from mismatch. These effects are a subject of future study.

Figure 7 shows the amplitude growth rates of the slow waves for different beam parameters and wall resistances. Note that the beam current and the geometry factor g, which depends on the ratio of the beam radius to the pipe radius, differ for each data point. A similar plot for the decay of fast waves is shown in Fig. 8. These figures show that the amplitude changes of localized space-charge waves passing through a resistive channel are in agreement with our theoretical predictions from Eq. (2), and smaller than the values predicted by the limiting case of Eq. (1).

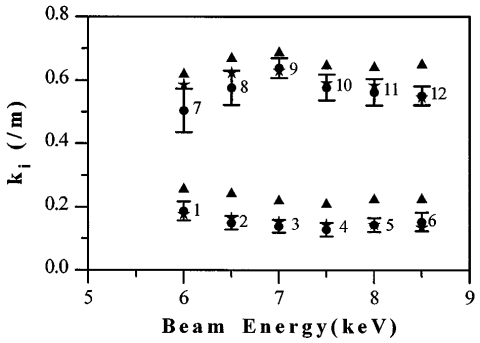

FIG. 8. Amplitude decay rate of fast waves with trapezoidal perturbation wave forms, where the dots with error bars represent the experimental results, the stars are from the Fourier analysis, and the triangles are from Eq. (1). The data points 1–6 are from the 5.44 kΩ tube, while the data points 7–12 are from the 10.1 kΩ tube.

In conclusion, resistive-wall instability experiments have been performed for the application in high-current particle accelerators. The experiments have demonstrated the growth of localized slow space-charge waves and the decay of fast waves in the long-wavelength range. The growth/decay rates of the instability have been measured in this new parameter regime. The theoretical analysis of the evolution of the pulse shape in the resistive channel based on Fourier transforms shows good agreement with the measurement, except for edge effects, where the distributed capacitance plays a role and the electrostatic long-wavelength assumption may break down. We have found that the amplitude change of localized space-charge waves due to the instability is smaller than that calculated from the conventional growth rate formula of Eq. (1), which has been commonly used to estimate the growth of the longitudinal instability in high current accelerators.

This research is supported by the U.S. Department of Energy.

[1] W. C. Hahn, Gen. Electr. Rev. **42**, 258 (1939).
[2] S. Ramo, Phys. Rev. **56**, 276 (1939).
[3] C. K. Birdsall, G. R. Brewer, and A. V. Haeff, Proc. IRE **41**, 865 (1953).
[4] V. K. Neil and A. M. Sessler, Rev. Sci. Instrum. **36**, 429 (1965).
[5] See, for example, M. Reiser, *Theory and Design of Charged Particle Beams* (Wiley, New York, 1994), see, Section 6.3 for a review and references.
[6] S. Humphries, Jr., J. Appl. Phys. **51**, 2338 (1980).
[7] E. Lee, in Proceedings of the 1981 Linear Accelerator Conference, Santa Fe, NM, 1981, edited by R. A. Jameson and L. S. Taylor (Los Alamos National Laboratory, Los Alamos, 1982), p. 263.
[8] J. Bisognano, I. Haber, L. Smith, and A. Sternlieb, IEEE Trans. Nucl. Sci. **NS-28**, 2513 (1981).
[9] P. J. Channell, A. M. Sessler, and J. S. Wurtele, Appl. Phys. Lett. **39**, 359 (1981).
[10] I. Hofmann, Z. Naturforsch **37A**, 939 (1982).
[11] D. A. C. Miller, Ph.D. thesis, University of California, 1994 (unpublished).
[12] See, for example, Chapter 1 of Ref. [11], and references therein.
[13] J. G. Wang, H. Suk, D. X. Wang, and M. Reiser, Phys. Rev. Lett. **72**, 2029 (1994).
[14] J. G. Wang, M. Reiser, W. M. Guo, and D. X. Wang, Part. Accel. **37–38**, 181 (1992).
[15] J. G. Wang, D. X. Wang, H. Suk, and M. Reiser, Phys. Rev. Lett. **74**, 3153 (1995).
[16] J. G. Wang, D. X. Wang, and M. Reiser, Phys. Rev. Lett. **71**, 1836 (1993).
[17] J. G. Wang and M. Reiser, Phys. Fluids B **7**, 2286 (1993).